SIMULATION AND PLANNING OF COCHLEAR IMPLANT SURGERY

FANG CHUANWANG

A REPORT SUBMITTED FOR THE MASTER OF COMPUTING

PROJECT

SCHOOL OF COMPUTING

NATIONAL UNIVERSITY OF SINGAPORE

Advisor:

Associate Professor LEOW Wee Kheng

Examiner:

Associate Professor LEOW Wee Kheng

Abstract

Hearing loss is a widespread health problem that causes inconvenience in patients' daily lives and impairs their cognitive functions. Cochlear implant surgery is an effective means of restoring hearing. The surgery requires precise drilling in temporal bone to avoid damaging important structures such as the facial nerve. However, due to individual differences in ear anatomy, surgical simulation using a standard skull model does not help much to improve the success rate of the surgery. The goal of this report is to use actual CT images to build a patient-specific ear model and develop a simulation tool to help surgeons accurately plan surgical paths and reduce uncertainty during surgery. The author used 3D Slicer to process CT data to generate a three-dimensional ear structure model and constructed a volumetric mesh through the SegmentMesher plug-in in 3D Slicer. Subsequently, a drilling simulator was developed that supports simultaneous import, rendering, interaction, and cutting of face, skull, safe zone models, and landmark points. Through simulation experiments on different patients, it is found that patient-specific models can more accurately reflect the patient's ear anatomy and help identify difficulties that may be encountered during surgery. Especially in patients with abnormal anatomical ear structures, simulation tools can help surgeons identify potential risks in advance, optimize surgical plans, and ensure patients' intraoperative safety and postoperative effects. This study provides an effective preoperative simulation and planning tool for cochlear implant surgery, which will help improve the accuracy and success rate of cochlear implant surgery. Future work will focus on improving image segmentation and modeling methods and integrating advanced surgical path planning algorithms into simulation software to further optimize surgical simulation and planning.

1 Introduction

1.1 Motivation

Hearing loss is particularly common among the elderly. A study conducted in the United States showed that 79.4% of the elderly with dementia also had hearing loss, and the incidence of hearing loss increased significantly with age[1]. In addition, a study conducted in Nigeria showed that 83.4% of older adults suffered from presbycusis, a condition that significantly reduced their quality of life and social skills[2]. However, hearing loss is not limited to the elderly population, but is a health problem that exists across age groups, and children and adolescents also widely suffer from it. A study conducted in Brazil conducted hearing tests on 646 students aged 2-15 years old, and the results showed that 29.5% of the students had hearing loss[3].

Hearing loss can have a number of adverse effects on patients' basic daily lives, such as work efficiency and interactions between family members. Studies have found that many patients have great difficulties in carrying out daily life activities, which leads to a decrease in their quality of life[2]. Hearing loss not only affects the ability to communicate in daily life, but can also lead to loneliness, depression and social isolation. For example, in a study conducted in Jordan, hearing loss was considered a neglected public health issue, and many affected people suffered negative psychological and educational effects[4]. In children and adolescents, there was a significant relationship between hearing loss and poor academic performance ($p = 0.0000$)[3]. This suggests that hearing problems are very likely to have a negative impact on the academic performance of children and adolescents. In the elderly population, a 6-year follow-up study of cognitive impairment in 1984 elderly people with an average age of 77.4 years showed that individuals with baseline hearing loss (pure-tone average $> 25dB$) had a 41% and 32% higher decline in Modified Mini-Mental State (3MS) and Digit Symbol Substitution test (DSS) scores than individuals

with normal hearing[5]. This decline in cognitive ability is likely to be organic, that is, accompanied by changes in brain physiological structure. A study found that hearing loss is associated with reduced volume in the temporal cortex, hippocampus, inferior parietal lobe, and precuneus[6]. The hearing-impaired have a faster rate of whole-brain atrophy, and the worse the hearing, the faster the hippocampus atrophies[7]. These organic changes may be one of the potential mechanisms by which hearing loss affects cognitive function.

Cochlear implant surgery has become a life-changing surgery for patients with severe hearing loss, which is able to restore hearing in many cases. One study found that most patients who received cochlear implants achieved open-set speech perception (79.2%) or environmental sound awareness (6.8%) after surgery[8]. Another study showed that patients who received cochlear implants had significant improvements in speech perception in noise in all spatial configurations[9]. In addition to restoring hearing, cochlear implant surgery also has significant cognitive benefits. A study of adult cochlear implant recipients showed that 12 months after implantation, patients had significant improvements in multiple cognitive subdomains, including attention, memory, and verbal fluency[10]. For the elderly patient population, one study suggests that this surgery may help slow cognitive decline and improve quality of life for elderly patients[11].

While the basic anatomy of the ear is similar in everyone, the precise morphology and location of the internal structures of the ear, such as the cochlea and surrounding bone, vary greatly. Due to this anatomical difference, it is impractical to use standard head skin models and standard skull models for simulation of cochlear implant surgery, especially when dealing with delicate structures such as the inner ear. As shown in the figure 1, the axial views of skull models of patients codenamed 20221116 and 20240806 are shown. It can be easily found that there are many differences between the ear bones of 20221116 and 20240806.

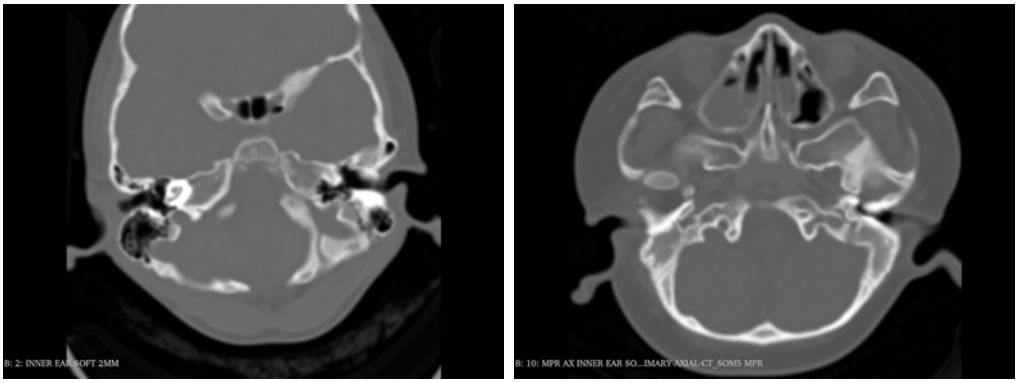

(a) 20221116 (b) 20240806

Figure 1: By comparing the ear bone models of two patients: **(a)** 20221116 and **(b)** 20240806, it can be found that there are many differences between the two. Therefore, for cochlear implant surgery, which requires extremely high precision, using a standard skull model for surgical simulation is not very helpful for the formulation of surgical plans.

Cochlear implant surgery requires precise drilling of the temporal bone to access the inner ear and correctly implant the device, while avoiding damage to important structures such as the facial nerve, consequently preventing complications such as facial nerve paresis[12]. Accurate simulation and planning of the drilling path are crucial to the success of the operation, and there are many related studies dedicated to achieving this goal[13, 14, 15, 16]. Drilling errors during surgery may lead to excessive bone removal, which may reduce the structural strength of the skull and cause implant instability[17]. Excessive bone cavity volume formed during surgery can also affect implant fixation and lead to postoperative complications such as cerebrospinal fluid leakage, electrode extrusion, and magnet migration[17].

1.2 Project Objective

This project aims to develop a surgical simulation tool for simulating and planning cochlear implant surgery. It consists of two main parts: (1) constructing a patient-specific ear model, and (2) simulating cochlear implant surgery. In detail, the objective of this project include:

1. Constructing various parts of the ear model, including skin, bones, and

other important organs, by segmenting the patient's CT images. Using patient-specific CT image data, the unique anatomical features of each patient's ear structure (such as the cochlea and surrounding bones) can be captured. This personalized model construction helps to accurately plan the surgical path, evaluate the feasibility of the surgical plan, and provide a basis for subsequent surgical simulation.

2. Simulate skin incision and bone drilling to reveal the internal structure of the ear. The simulation tool developed in this project can help surgeons determine the precise location of resection, minimize unnecessary removal, and avoid damage to important organs, in this way helping surgeons better plan surgical paths and reduce uncertainty during surgery. By visualizing the patient's specific anatomical structure in 3D, doctors can optimize implant placement and enhance the stability of the patient's implant.

2 Anatomy of the Ear

Cochlear implants (CI) bypass damaged ear structures and use electrical stimulation to directly act on the auditory nerve fibers in the cochlea, allowing sound signals to be transmitted to the brain to replace the function of damaged cochlear hair cells, as a result helping hearing-impaired people restore some of their auditory perception abilities. This process requires inserting electrodes into the cochlea and firmly placing the implant in a suitable position.

The human ear consists of three parts: the external ear, the middle ear, and the inner ear, as shown in the figure 2 and the position in the CT image in the figure 3. The outer ear is the first part of the ear, which is mainly composed of the auricle and the external auditory canal. Cochlear implant surgery usually starts with the skin behind the auricle. The middle ear is an air-filled chamber that contains three ossicles: the malleus, the incus, and the stapes. These three

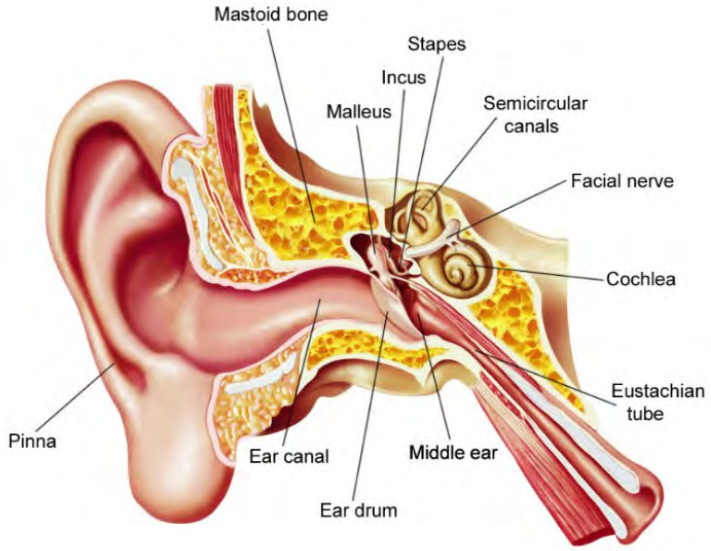

Figure 2: Diagram of the human ear anatomy[18]: The diagram shows the main structures of the human ear, including the external ear, middle ear, and inner ear. The external ear is responsible for collecting and guiding sound, the middle ear converts sound waves into vibrations and amplifies sound signals, and the cochlea of the inner ear is responsible for converting vibrations into electrical signals and transmitting them to the auditory nerve.

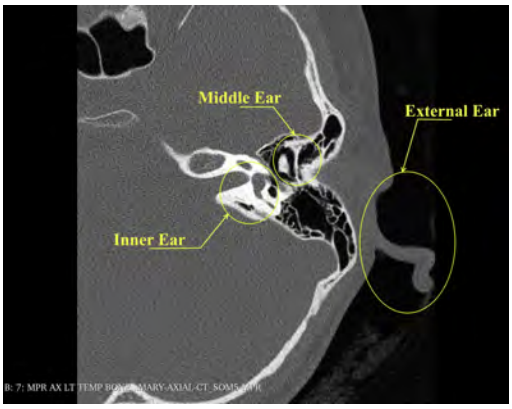

Figure 3: Schematic diagram of the location of the outer ear, middle ear and inner ear in CT images: The specific locations of the outer ear, middle ear and inner ear are marked in CT images to help understand the actual anatomical distribution of each part in the auditory system.

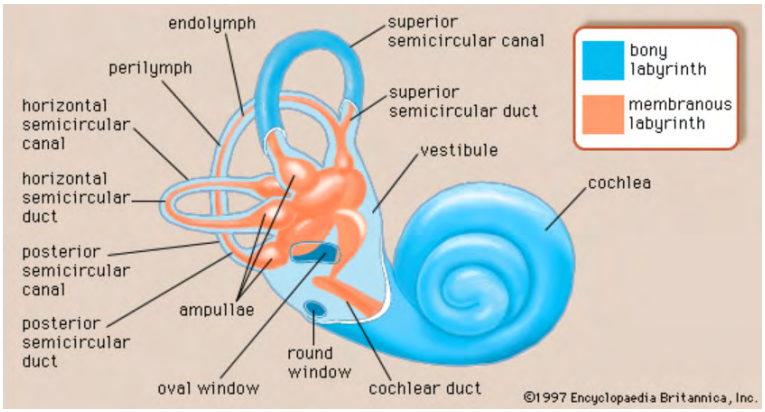

Figure 4: Inner ear anatomy diagram[19]: shows the structure of the inner ear, mainly including the vestibule, semicircular canals and cochlea.

tiny bones form a chain connecting the eardrum to the oval window of the inner ear. Cochlear implant surgery needs to avoid damaging the ossicles when performing bone drilling. The inner ear is the most complex part of the auditory system, mainly composed of the vestibule, semicircular canals, and the cochlea. Its anatomical structure is shown in the figure 4. The cochlea is a spiral, fluid-filled structure similar to a snail shell, with a membrane inside that divides it into three fluid-filled channels.

The area of the ear that is the focus of cochlear implant surgery is the inner ear, with the cochlea being the most important area of the surgery. The unique spiral shape and delicate structure of the cochlea require extremely careful handling during the implantation process. During surgery, the implant electrode array needs to be inserted into the cochlea with minimal trauma to preserve any residual hearing. Figure 5 shows how the cochlear implant electrode is inserted into the patient's cochlea through the round window. Even small anatomical differences in the size or curvature of the cochlea can differentiate the insertion process, which further increases the need for customized simulation models. Important structures in the cochlea include the basal turn and the various scala of the cochlea, especially the round window. The round window is an opening in the wall of the cochlea covered by a thin membrane, the round window membrane, which compensates for the movement of fluid within the cochlea. The

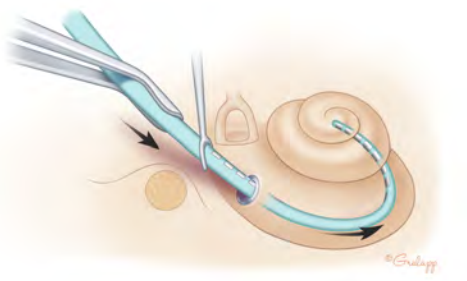

Figure 5: Once the round window is found, the surgeon can insert the electrode array of the cochlear implant into the inner ear through the round window[20].

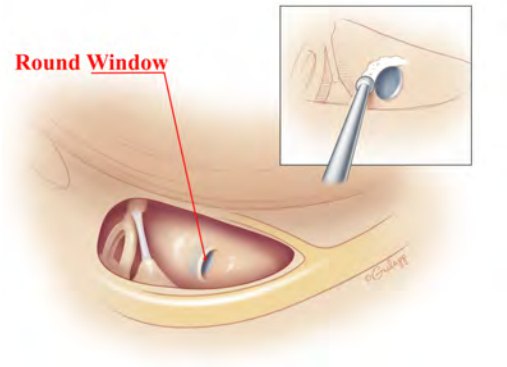

Figure 6: Cochlear implant surgery requires the incision or removal of some soft tissue and bone structure to expose the round window[21].

appearance of the round window and the round window membrane is shown in Figure 6. Figure 7 and Figure 8 show the location of the round window in the left ear of patients codenamed 20221116 and 20240806, respectively. In many cochlear implant surgeries, the round window is the entry point for the electrode array to be inserted into the cochlea. In some cases, if the view through the round window is obstructed, a stoma may be made in the tympanic recess of the cochlea. The facial nerve also needs to be identified and protected during surgery. The facial nerve is close to the cochlea and temporal bone and controls the muscles of the face. Figure 9 and figure 10 show the location of the facial nerve in the left ear of patients 20221116 and 20240806, respectively. If there is a surgical error during the operation, damages may be caused to the facial nerve, resulting in facial paralysis or weakness. The operation near the vestibular system during the operation also requires special care. The vestibular system

Figure 7: The location of the round window and nearby structures in the left ear of patient codenamed 20221116 show the standard anatomical structure suitable for the insertion of the electrode array.

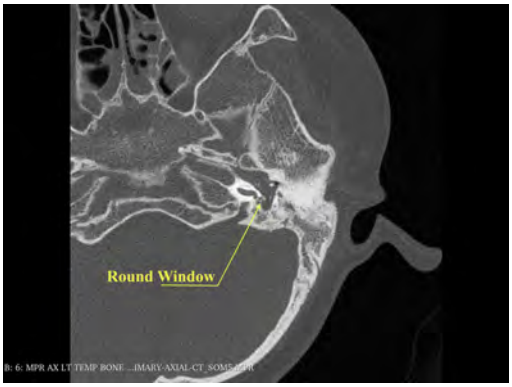

Figure 8: The location of the round window and nearby structures in the left ear of patient codenamed 20240806 show that the round window field of view is obstructed and a stoma may be needed in the tympanic recess of the cochlea.

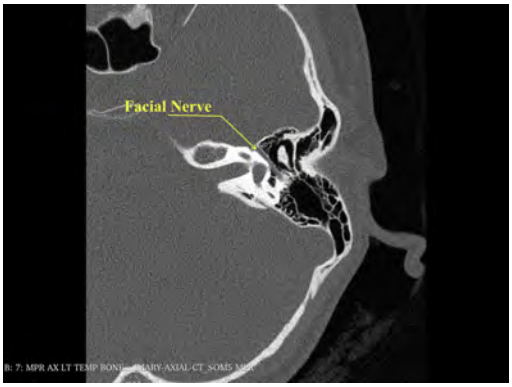

Figure 9: The location of the facial nerve in the left ear of a patient codenamed 20221116 and its nearby structures, which shows the normal anatomical relationship between the facial nerve, cochlea and temporal bone.

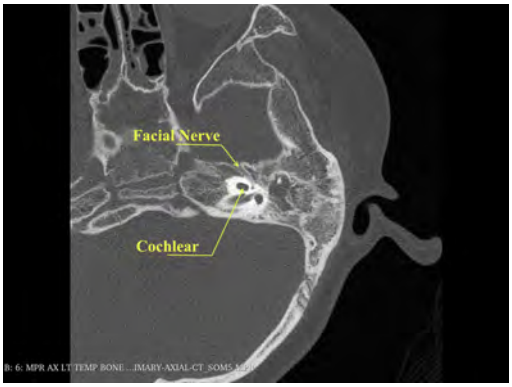

Figure 10: The location of the cochlear and facial nerve in the left ear of patient codenamed 20240806.

is located near the cochlea and controls balance. It is composed of semicircular canals and otolith organs. Drilling near the vestibular system risks inducing balance disorders.

3 Related Work

Peter Trier et al[22]. developed a virtual reality simulator called Visible Ear Simulator (VES), which is equipped with a Geomagic Touch haptic device that provides force feedback. This force feedback function allows users to feel tactile feedback when performing virtual surgical operations, thus enhancing the realism of the simulation. VES has a dedicated cochlear implant module to simulate the drilling and electrode implantation process in cochlear implant surgery, providing users with a realistic surgical experience. However, although VES provides a highly simulated surgical environment, it is not patient-specific, which means that it fails to fully replicate each patient's unique anatomy and surgical needs.

Blake Jones et al[23]. used images from synchrotron radiation phase contrast imaging (SR-PCI) to create a high-resolution human cochlear model and developed a simulator using Unity3D specifically for simulating the process of electrode insertion into the human cochlea. Although this work provides an in-depth simulation of the electrode insertion process, it does not cover the sim-

ulation and planning of cochlear implant surgery starting with skin resection and bone removal. It is worth noting that although SR-PCI technology played an important role in this work, its high cost precludes routine clinical use. In contrast, CT scanning is more common in common clinical practice due to its relatively low equipment and operating costs.

Rebecca L. Turok et al[24]. developed a cochlear implant placement simulator that integrates an interactive 3D visualization environment and a controller with tactile feedback, which allows the surgical technique and patient anatomy to be adjusted in simulation to study surgical outcomes under different conditions. They designed an experiment specifically to compare the force distribution on the inner ear anatomy when two different surgical insertion methods are used, round window (RW) and tympanostomy (CO) techniques. However, the simulator does not simulate the drilling process and therefore cannot assist surgeons in drilling path planning.

Mario Ceresa et al[25]. proposed a framework for creating statistical shape models (SSM) and finite element models (FEM) based on patient-specific high-resolution μCT data. This framework performs electrical simulations of electromagnetic fields based on Maxwell's equations on patient-specific models, which includes implanted electrodes and nerve fibers, to predict voltage distribution and neural activation locations after electrode placement. This model aims to predict electrode crosstalk and neural activation at the electrophysiological level to optimize surgical outcomes and improve the functional output of cochlear implant surgery. Although this study used a patient-specific model, it focused on the simulation of electromagnetic fields and prediction of neural activation and did not involve simulation of mechanical factors such as the drilling process, bone tissue removal, and surgical path planning.

Olivier Goury et al[26]. numerically simulated the behavior of electrodes mechanically inserted into cochlear implants during surgery using the finite element method (FEM) and the Simulation Open Framework Architecture (SOFA)

framework. They used a patient-specific cochlear geometry model for simulation to show the impact of the clinical parameter of insertion angle on the forces on the cochlear wall and basilar membrane and postoperative trauma. In addition, they analyzed a variety of parameters that affect the simulation results, including mechanical parameters (such as friction, implant stiffness, membrane elasticity, etc.) and clinical parameters (such as insertion angle), and specifically studied the impact of the friction coefficient on surgical outcomes. This study simulated the behavior of the electrodes during mechanical insertion into the cochlear during surgery and did not cover the path planning of the drilling process during cochlear implant surgery.

In summary, existing studies have made important progress in simulation of cochlear implant surgery, which mainly includes virtual reality simulation of surgical experience, simulation of electrode insertion process based on high-resolution imaging, simulation of adjustable anatomical structure combined with force feedback, and statistical shape and electrophysiological models based on patient-specific data. However, these studies have some shortcomings: lack of individual patient specificity, high imaging cost, and failure to simulate skin incision and bone removal processes. These studies are related to the goals of this project, but they are different. This project aims to develop a cochlear implant surgery simulator based on the individual anatomical structure of the patient, which can simulate the surgical process from skin incision to bone removal, in this way assisting doctors in drilling path planning to better meet the unique anatomical characteristics and surgical needs of each patient, and improve the accuracy and effectiveness of the surgery.

4 Cochlear Implant Surgery Simulation

4.1 Ear Model Construction

The construction of patient-specific ear models involves segmenting the skin, the bones and other relevant parts of the ear from a patients' CT images. When performing image segmentation, in the early stage of the project, this report uses the ITK-SNAP tool for segmentation, and then uses MeshLab to clean up the model. Specifically, the Active Contour (aka "Snake") Segmentation Model in ITK-SNAP is used for semi-automatic active contour segmentation. Threshold mode, Lower threshold, and Upper threshold are set by observing the image segmentation preview in the three views. Then add bubbles and perform bubble diffusion calculation. To be specific, in the 3D view, use the cross cursor to select the specified position within the target structure. Then initialize a bubble at the cursor position and adjust its size. Next, move the cursor to gradually add multiple bubbles on slices at different levels, and repeat this process to cover various parts of the target structure. After completing the bubble addition, enter the Evolution step and start the bubble diffusion calculation. Observe the diffusion in real time through the three views. When the diffusion process is close to the ideal coverage, the diffusion calculation can be stopped. At this time, observe the diffusion results and find the missing structure that has not been covered. If a missing area is found, return to the bubble addition step to add bubbles to the missing area. In actual operation, even after multiple bubble additions and diffusion calculations, there may still be areas with incomplete coverage. It is necessary to repeatedly perform a cycle of bubble addition and diffusion calculation until a satisfactory coverage result is obtained.

After modeling with ITK-SNAP, the model can be imported into the simulation tool for simulation. However, at this time, the model often has some defects, such as non-manifold edges, non-manifold faces, and unclosed holes. These defects will cause software-level exceptions when the cutting operation

is triggered. Therefore, the model must be cleaned and repaired before importing the simulation tool. For cleaning two-dimensional meshes, MeshLab is an ideal tool[27]. Therefore, after completing ITK-SNAP modeling, MeshLab needs to be used to clean and repair the mesh. Each round of cleaning and repair includes the following steps: deleting isolated components, detecting and merging duplicate vertices, deleting duplicate faces (i.e., faces composed of the same vertices), converting non-manifold edges to manifold structures through splitting vertices, filling holes, unifying face directions to ensure consistency, deleting faces with zero area, removing self-intersecting faces, recalculating vertex normals, and splitting polygonal faces into triangular faces, as a result converting the mesh into a pure triangular mesh. In actual operation, this report implemented a Python program to automate the entire repair process by calling the corresponding functions in the pymeshlab library to ensure that no step is missed, by which the model is cleaned efficiently. In the execution of the Python script, the cleaning and repair process is designed to be looped until the stop condition is met, that is, the number of vertices and faces before and after a round of cleaning has not changed, and there is no change in the number of vertices and faces before and after each step in this round.

However, in actual operation, it was found that there are some problems with the workflow of image segmentation based on ITK-SNAP combined with MeshLab cleaning and repair. First, when using ITK-SNAP for bubble diffusion calculations, the software often has difficulty capturing subtle structures. Therefore, after the diffusion is completed, it is often necessary to repeatedly return to the bubble addition step to supplement the missed bubbles, consequently increasing the complexity and time of the operation. Second, when using pymeshlab for cleaning, for some models, the script loop has not ended after running for several hours. After the first few rounds of cleaning, although the number of vertices and faces changes after each step of each round, these values remain unchanged in the same steps of adjacent rounds, forming a repetitive pattern. The

number of vertices and faces after each step in each round is always the same as the previous round, falling into an invalid loop. However, these cleaning steps cannot be omitted, otherwise they will cause software exceptions when simulating cutting. Therefore, for some models, this workflow based on ITK-SNAP image segmentation combined with MeshLab cleaning and repair is not applicable, which may lead to repeated iterations and unstable cleaning processes. In addition, the workflow based on ITK-SNAP for image segmentation combined with MeshLab cleaning and repair can only generate surface meshes, which are hollow and lack internal volume. After these surface meshes are cut in the simulation tool, the boolean operation function automatically adds surfaces to represent the newly exposed cut surface. However, in actual experiments, this process may introduce defects in the cut model, such as non-manifold geometries, which refers to the situation where the mesh topology is illegal, such as an edge shared by more than two faces, or there are incorrect intersections between faces. These defects will cause subsequent operations to trigger software-level exceptions, causing the simulation process to crash or produce incorrect results. In contrast, volumetric mesh can stably generate valid and legal geometric structures during the cutting process. This significantly improves the stability and reliability of the simulation and avoids exceptions caused by mesh defects.

Therefore, in the later stage of the project, this report uses the 3D Slicer tool for image segmentation and the SegmentMesher plug-in for volumetric mesh construction to deal with the above problems. In the image segmentation process, this report first performs a series of segmentation steps on each model (face model, skull model, and safe zone model) to ensure accurate extraction of the target area. First, in the three-view interface of 3D Slicer, select the axial view and navigate the slice to the appropriate level containing the anatomical structure of interest to accurately locate the target tissue. After locating the target tissue, image enhancement is required. This report uses the ”Select Region” tool in the Windowing function to select the region of interest and adjust the

window width and window level parameters. This image enhancement process can optimize the contrast of the target tissue and provide more intuitive visual support for the subsequent segmentation process. Next, in the threshold segmentation step, according to the grayscale value range of the anatomical structure, the Threshold Segmentation tool is used to set an appropriate threshold interval to preliminarily extract the target tissue, such as facial soft tissue, skull or safe zone. To further remove non-target areas or image noise, this report uses manual editing tools, including ”Scissors”, ”Eraser” and ”Islands” functions, to crop and check the model and remove unnecessary areas to increase the calculation speed during the simulation process.

The above segmentation steps are applied to the face model, skull model and safe zone model respectively. Subsequently, the Logical Operators tool is used to remove the parts of the face model that overlap with the safe zone, which includes important blood vessels and nerves, to avoid the phenomenon that the face model occludes the safe zone model in the simulation tool.

In the volumetric mesh construction process, this report uses the SegmentMesher plug-in to generate a three-dimensional volumetric mesh for each model. First, Cleaver[28] is selected as the mesh generation method in the plug-in. The Cleaver tool is based on the Lattice Cleaving[29] algorithm, which can handle volume domains containing any number of materials, which is very useful for biomedical simulation scenarios. Meanwhile, the tetrahedral mesh generated by the Lattice Cleaving algorithm has bounded dihedral angles, which means that the quality of the mesh elements is guaranteed[29]. Compared with TetGen[30], Cleaver is specifically designed to handle complex geometries and can better capture the details of models involved in this project[29].

After selecting the Cleaver method, there is a need to adjust the key parameters of the Cleaver algorithm, including feature scaling, sampling rate, and rate of change of element size, according to the complexity of different models and simulation requirements. The feature scaling ranges from 0.2 to 5.0, and the

default value is 2.0. Increasing the feature scaling will generate larger mesh elements, which can reduce the amount of calculation. Conversely, reducing this parameter can generate a finer mesh, which helps capture subtle anatomical details. The sampling rate ranges from 0.1 to 1.0, and the default value is 0.2. Increasing the sampling rate will increase the resolution of the mesh and more accurately depict complex structures; reducing the sampling rate will result in a coarser mesh, which is suitable for scenarios where the model size needs to be reduced. The rate of change of element size ranges from 0.0 to 1.0, and the default value is 0.2. Reducing the rate of change of element size ensures a smooth transition of the grid cell size between different regions, but may ignore some small, rapidly changing features; in contrast, increasing this parameter will increase the transition difference of the cell size, thus helping to form a finer grid in the detail area and maintain a coarse resolution in other areas. The volume grid construction in this project adopts the Cleaver method, and different parameters are applied to the face model, skull model and safe zone model for volume grid generation to meet the different fineness requirements of each model.

However, there are still some subtle structures that are difficult to accurately present in the volumetric mesh. The round window of the inner ear is a typical case. Even if the highest accuracy calculation parameters is applied when using the Cleaver method for volumetric mesh generation, it is still impossible to fully capture the details of the round window.

To address this limitation, the author manually finely marked the round window structure during the image segmentation stage. Specifically, the author used the Markups function to add a series of landmark points on each layer of the tomographic image in the axial view to outline the outline of the round window. This manual delineation method ensures that the round window structure can be clearly identified when the progress of the simulated surgery reaches the inner ear. In this way, we improved the accuracy of identifying key anatomical structures during simulated surgery and enhanced the reliability and authenticity of

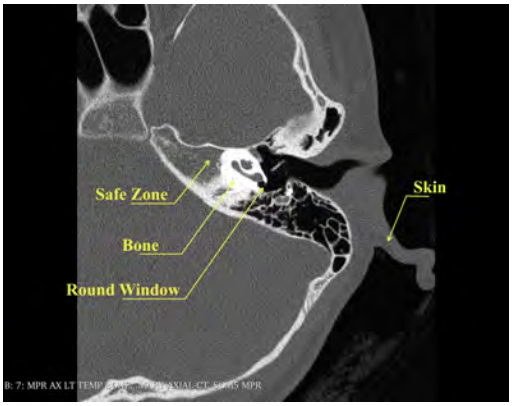

Figure 11: CT images of the anatomy of the skin, bones, safe zone (including important blood vessels and nerves), and round window in patient code 20221116.

Figure 12: Representation of skin in a volumetric mesh.

the simulation.

Figure 11 shows the anatomical structures of the skin, bones, and safe zone (including important blood vessels and nerves) in the CT image of the patient codenamed 20221116. Through image segmentation and volumetric mesh construction, the author obtained the corresponding three-dimensional model. Among them, the volumetric mesh model of the skin is shown in Figure 12; the volumetric mesh model of the bone is shown in Figure 13; the volumetric mesh model of the safe zone is shown in Figure 14; and the landmark points of the round window structure are shown in Figure 15.

4.2 Surgery Simulation Tool

This report implements a drilling simulator, which aims to provide surgeons with a simulation and planning tool for cochlear implant surgery. Through this simulator, surgeons can simulate cutting and observing the bones, skin and other

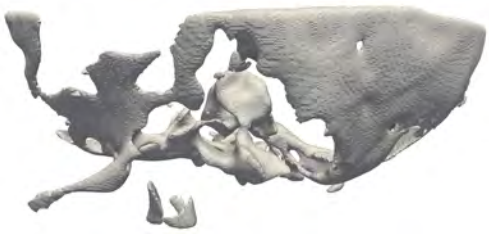

Figure 13: The representation of bones in a volumetric mesh.

Figure 14: Representation of safe zone, including important blood vessels and nerves, in a volumetric mesh model.

Figure 15: Representation of the marker points of the round window structure.

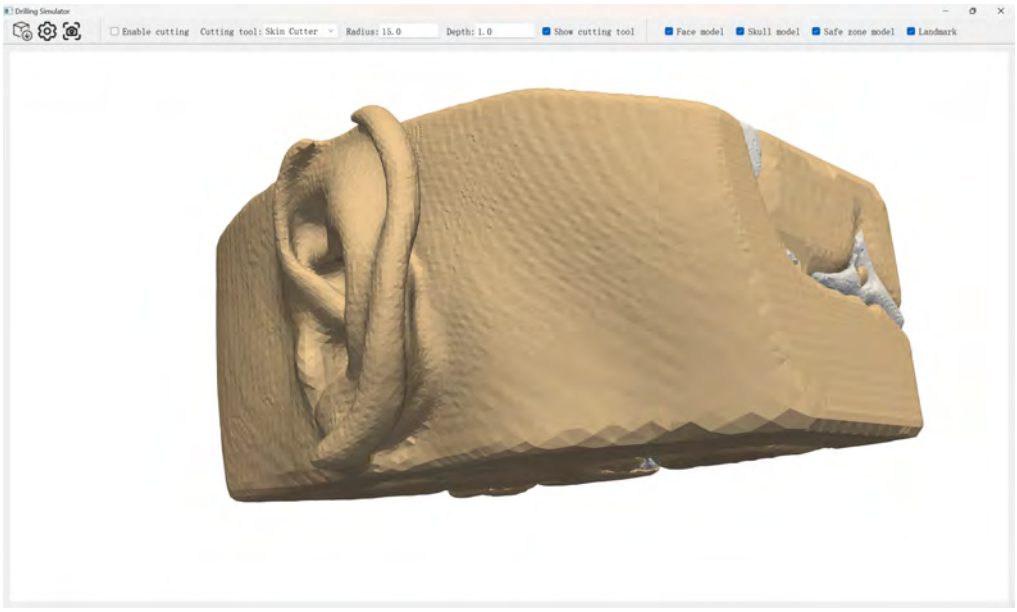

Figure 16: Overall GUI of the simulator.

parts involved in the operation. This simulator supports the simultaneous import, rendering, interaction and cutting of the face model, skull model and safe zone model. It has strong visualization and user interactivity, and can effectively assist surgeons in planning the operation steps of cochlear implant surgery.

This simulator is developed and implemented using Python 3.11.9. To ensure the reproducibility and compatibility of the environment, all necessary Python packages and their corresponding versions are listed in the table 1. This table comprehensively lists all the dependencies required for the simulator to run, ensuring that the software environment can be accurately reproduced in testing and subsequent development.

The overall graphical user interface (GUI) of this simulator is shown in Figure 16. The toolbar at the top of the interface provides convenient function access and is divided into three areas: left, middle, and right.

The left side of the toolbar contains three buttons: model import panel, setting panel, and screenshot button. The model import panel is used to load the model required for simulation, as shown in Figure 17; the setting panel allows users to access and adjust the various parameters of the simulator, as shown in Figure 18; the screenshot button allows users to capture the screen image of the

Table 1: All Python packages and their versions used by the simulator in this project.

Package	**Version**
altgraph	0.17.4
certifi	2024.8.30
charset-normalizer	3.4.0
contourpy	1.3.0
cycler	0.12.1
fonttools	4.54.1
idna	3.10
kiwisolver	1.4.7
matplotlib	3.9.2
mpmath	1.3.0
numpy	2.1.2
packaging	24.1
pefile	2023.2.7
pillow	11.0.0
platformdirs	4.3.6
pooch	1.8.2
pyinstaller	6.11.0
pyinstaller-hooks-contrib	2024.9
pyparsing	3.2.0
PyQt5	5.15.11
PyQt5-Qt5	5.15.2
PyQt5_sip	12.15.0
python-dateutil	2.9.0.post0
pyvista	0.44.1
pyvistaqt	0.11.1
pywin32-ctypes	0.2.3
QtPy	2.4.1
requests	2.32.3
scooby	0.10.0
sip	6.8.6
six	1.16.0
sympy	1.13.3
typing_extensions	4.12.2
urllib3	2.2.3
vtk	9.3.1

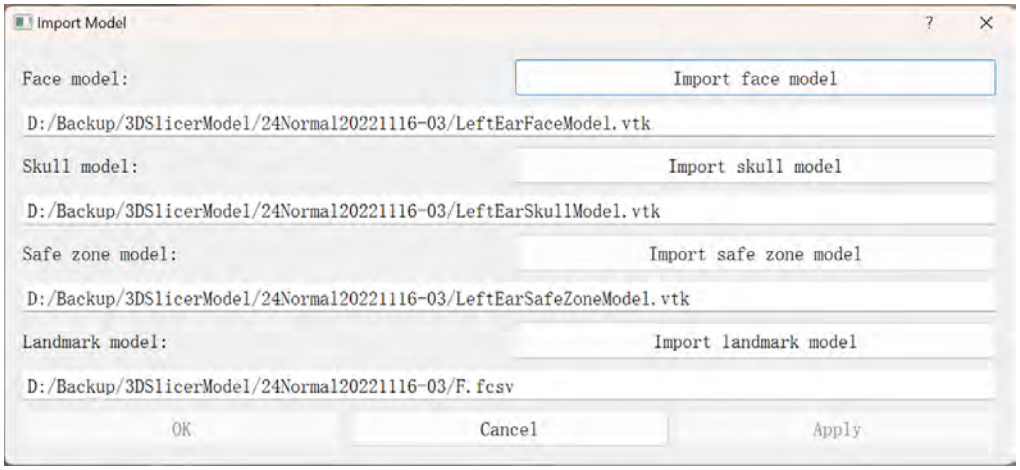

Figure 17: Model import panel of the simulator.

current simulation state at any time. After clicking, the current scene can be screenshoted and a successful prompt will be returned, as shown in Figure 19.

The middle area of the toolbar provides common settings for the cutter. Users can adjust the main parameters and behaviors of the cutting tool here to achieve precise operation and interaction with the model to meet different simulation needs. This simulation software provides the two most commonly used cutting tools in Cochlear implant surgery: Skin Cutter and Diamond Burr.

There are checkboxes on the right side of the toolbar to control the visibility of each model. Users can display or hide specific models by checking or unchecking, which helps to focus on specific components or simplify the view, thereby improving the efficiency and flexibility of simulation operations.

Other detailed setting options are located in the settings panel. This panel provides comprehensive control over the functions of the simulator, including the adjustment of colors of models, opacity of the cutting tool preview, etc., to meet the user's refined needs for the simulation process.

This simulator allows users to import three models simultaneously: face model, skull model and safe zone model. These models are imported as UnstructuredGrid objects of the PyVista library, which are displayed and interacted with the user interface through PyQt5. The 3D model is read, rendered and cut through pyvista and vtk (Visualization Toolkit) libraries, which achieves effi-

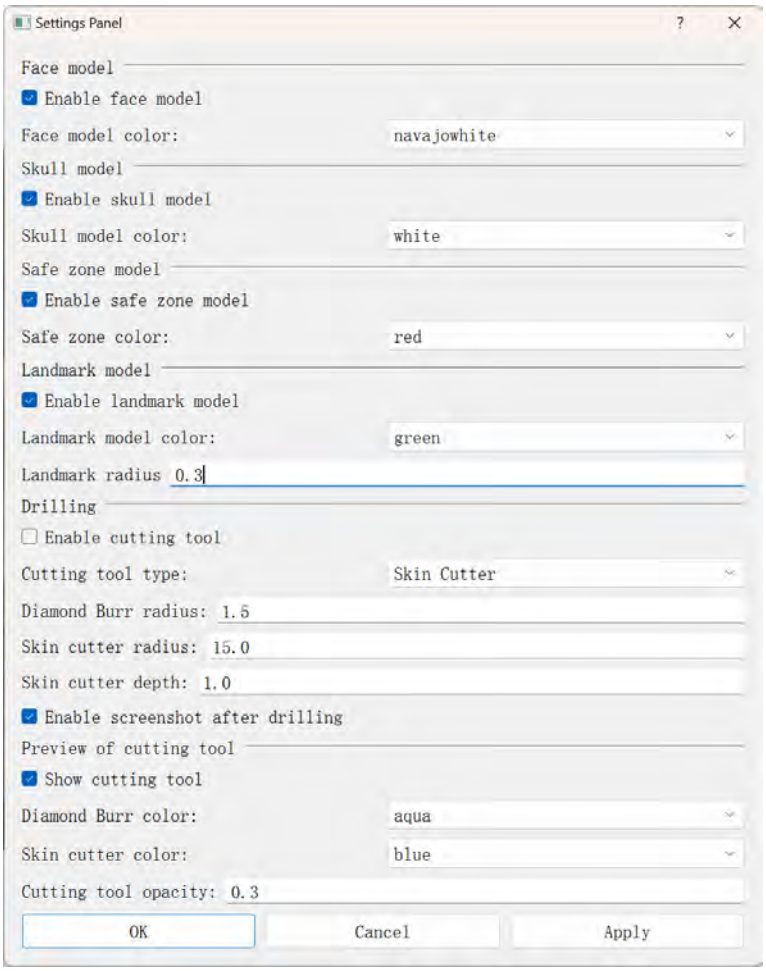

Figure 18: Settings panel of the simulator.

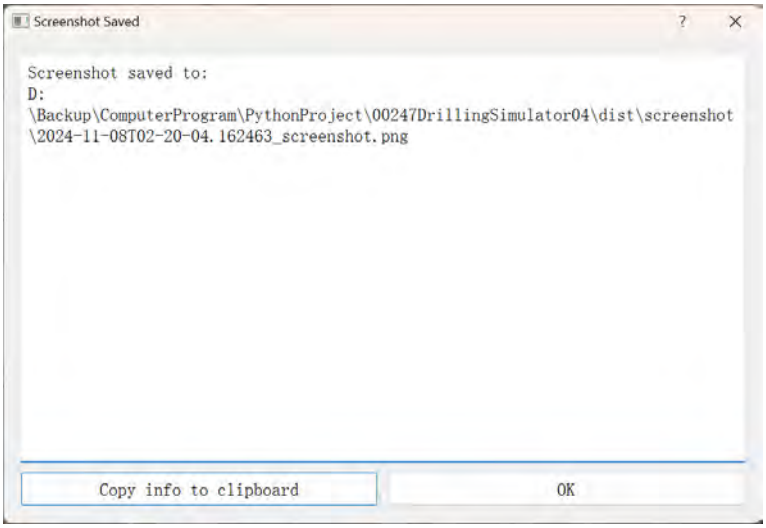

Figure 19: The successful screenshot pop-up window of the simulator.

cient 3D data processing and rendering.

In order to provide an intuitive and flexible interaction method, the simulator supports the following user operations:

- Rotate the view: Hold down the left mouse button and drag to rotate the model, so that the surgical area can be observed from different angles.
- Zoom the view: Scroll the mouse wheel to zoom in or out of the model, so that details or the overall structure can be viewed.
- Pan the view: Hold down the Shift key and drag the left mouse button to pan the view in order to quickly locate the area of interest.

These methods are consistent with the interaction logic of most 3D visualization software, in doing so allowing users to quickly get started and operate intuitively.

The simulator provides the ”Show Cutting Tool” function, which is mainly to help surgeons intuitively preview the area that the current cutting operation will affect before the actual cutting. Through the preview, users can see the shape of the tool and its position on the model, so as to adjust the cutting parameters (such as radius, depth) to meet the surgical needs and avoid accidental damage to important structures.

In order to achieve real-time and efficient cutting tool preview function, the simulator adopts the following steps to implement the function:

1. Get the mouse screen position and camera information: Use mouse events to get the mouse position coordinates (x, y) on the screen. At the same time, get the camera position and viewing angle information of the current renderer, including the camera position and projection direction.
2. Calculate the ray from the camera to the position pointed by the mouse: Through the renderer's SetDisplayPoint and DisplayToWorld methods, the screen coordinates are converted to world coordinates to obtain two

points (world_point_near, world_point_far) of the ray on the near clipping plane and the far clipping plane. Then, calculate the ray direction vector: ray_direction = world_point_far - world_point_near, and perform normalization.

3. Use OBB tree to get the nearest intersection point: In order to efficiently find the nearest intersection point between the ray and the model in the 3D model, the OBB tree (Oriented Bounding Box Tree) data structure in the vtk library is used. For each enabled model (face model, skull model, safe zone model), this simulator will build a corresponding OBB tree to speed up spatial queries. When it is necessary to obtain the intersection point, this simulator uses the IntersectWithLine method to intersect the ray with the OBB tree to obtain the nearest intersection point.

4. Get the view direction: Get the projection direction from the camera to get the view direction vector, view_direction, for subsequent positioning and rendering of the cutting tool.

5. Update the rendering of the cutting tool: According to the current cutting tool type (diamond burr or skin cutter), update the position and shape of the corresponding cutting tool model respectively. For the diamond burr, use vtkSphereSource to create a sphere with the center at the nearest intersection and the radius as the set cutting radius. For the Skin Cutter, vtkLineSource and vtkTubeFilter are used to create a cylinder. The start and end points are calculated based on the nearest intersection point and the view direction vector view_direction, and the length is the set cutting depth.

Through the above steps, the preview of the cutting tool is updated in real time when the user moves the mouse, so that the surgeon can intuitively see the upcoming cutting area.

In the initial implementation, this report used vtkCellPicker to obtain the

model surface point corresponding to the mouse position. However, vtkCellPicker has poor performance when processing large 3D models, and a single picking operation takes about 2 to 3 seconds. Since the frequency of mouse movement events is usually around 100 Hz, such time consumption cannot meet the requirements of real-time rendering.

To solve this problem, this report utilizes vtkOBBTree. OBB tree is a space segmentation data structure. By constructing OBB tree, the 3D space can be recursively divided into smaller bounding boxes, each of which contains a part of the model geometry. In the process of finding the intersection point between the ray and the object, the intersection of the ray and the bounding box is first checked. Only when they intersect, the intersection with the geometry in the bounding box is further calculated. In this way, by excluding a large number of spatial areas that cannot intersect, the amount of calculation is significantly reduced and the intersection speed is improved. In contrast, vtkCellPicker needs to traverse all cells when processing complex models, which has a large amount of calculation and thus has low performance. After using vtkOBBTree, the time taken for a single intersection operation is reduced to about 0.03 seconds, successfully meeting the performance requirements of real-time preview.

One of the core functions of the simulator is to cut the model to simulate the drilling and cutting operations in real surgery. The implementation steps of the cutting function are as follows:

1. Get the cutting position and direction: Use the same method as the preview function to get the world coordinates and viewing direction of the nearest point on the model surface corresponding to the mouse position.

2. Set the Clip Function according to the currently selected cutting tool: If it is a diamond burr, use vtkSphere as the clipping function, set the center of the sphere as the cutting point, and the radius is the set drill radius. If it is a skin cutter, use vtkCylinder and vtkPlane to form a cylinder of finite length. Set the axis of the cylinder as the viewing direction, and the

radius as the set cutter radius. Then use two planes to limit the length of the cylinder to form a finite length cylindrical area.

3. Perform model clipping: Use vtkClipDataSet to operate the model with the clipping function, remove the geometry inside the clipping function, and realize the cutting of the model.

4. Update the model and OBB tree: Finally, update the clipped model data to the renderer and refresh the display. Then extract the surface mesh of the new model to reconstruct the OBB tree of the corresponding model to ensure that in subsequent interactions, the ray-model intersection operation can find the intersection point on the correct new shape, in this way ensuring that the interaction operation is correct.

Through the above process, the simulator realizes real-time cutting of the model, and the surgeon can perform simulation operations as needed and observe the results after cutting.

In actual surgery, it is usually necessary to remove a large area of skin in the initial stage to expose the underlying bone structure. In order to simulate this process, the skin cutter in the simulator is designed to cut only the face model. This design allows surgeons to quickly remove the skin part and focus on the subsequent fine operation. Specifically, for the implementation of the skin cutter, the Drilling Simulator checks the current cutting tool type and target model during the cutting operation. When using the skin cutter, only the enabled face model is cut, ignoring the skull model and the safe zone model. In this way, the range of the skin cutter is controlled by logically limiting the cutting object.

The simulator allows surgeons to adjust the parameters of the cutting tool, including radius and depth, to meet different surgical needs. A larger radius can be used to quickly remove large areas of tissue, and a smaller radius is suitable for fine cutting operations. Depth is only applicable to the skin cutter, and the depth parameter determines the depth to which the cutting tool can cut into

the model. By adjusting these parameters, surgeons can choose the appropriate cutting tool settings according to the needs of different surgical stages to better simulate different operation steps in actual surgery.

In the implementation of this simulator, a safe zone model is specially introduced as an independent model for import and rendering. This indicates key areas that should be avoided from cutting during surgery, such as important nerves and blood vessels. Clarifying the safe zone in the simulation helps surgeons better plan the surgical path and ensure that surgical tools are away from critical areas, thereby improving the safety and success rate of the operation. The safe zone model is displayed together with the face model and skull model, and is marked by eye-catching colors. During the cutting operation, the safe zone model also participates in the construction and intersection calculation of the OBB tree.

This simulator provides a landmark display function. During image segmentation using 3D Slicer, users can export the marked landmarks as .fcsv (Fiducial CSV) files and then import them into this simulator. The landmark function helps to identify subtle structures that are difficult to accurately reconstruct in the model, or mark important anatomical areas. In addition, it can also indicate the stage of the surgical process and provide navigation and reference for the surgeon.

In addition to the screenshot button provided in the toolbar, the simulator also automatically takes a screenshot after each cutting operation by default (this function can be disabled in the settings panel) to automatically record the key steps and important operations during the simulation process. With these functions, the simulator can more comprehensively support surgical simulation and provide more intuitive and detailed operation records.

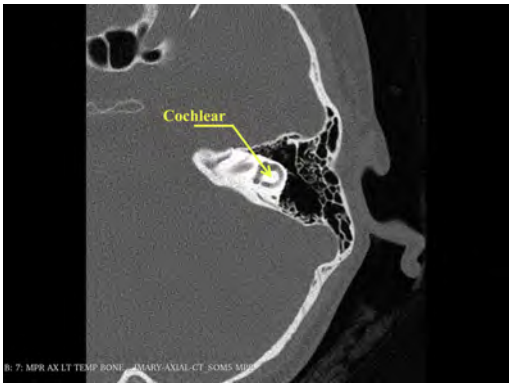

Figure 20: The cochlea and nearby structures of patient codenamed 20221116.

4.3 Simulation Results

The section illustrates the results of model construction and surgery simulation on two subjects, namely normal subject 20221116 and abnormal subject 20240806. For each subject, the results for the left ear and right ear are illustrated. These examples display the differences between typical and challenging situations encountered in cochlear implant surgery. Through visualization, this report shows how anatomical differences affect the drilling process and the ability of the simulator to effectively guide surgical decisions.

Patient 20221116 has normal ear anatomy, and the axial tomographic image of the skull in the ear area is shown in Figure 1a. The cochlea and surrounding structures of this patient are shown in Figure 20; the facial nerve and its adjacent anatomical structures are shown in Figure 9; the round window and its surrounding tissue are shown in Figure 7. In contrast, patient 20240806 has abnormal ear anatomy, and the axial tomographic image is shown in the figure 1b. The cochlea and facial nerve and their surrounding structures of patient 20240806 are shown in the figure 10, and the round window and its adjacent tissue are shown in the figure 8.

By comparison, it can be found that patients with normal ear anatomy have large air spaces around the cochlea, facial nerve, and round window; while patients with abnormal anatomy have almost no air spaces around these key organs and tissue, but are filled with soft tissue and bone structures, which increases the

Table 2: The threshold setting for each CT data set during image segmentation.

	Face Model	Skull Model	Safe Zone Model
20221116	-369∼367	506∼2723	-349∼495
20240806	-367∼248	614∼3071	-366∼603

Table 3: Parameter settings for constructing volumetric meshes using the Cleaver method for each CT dataset for the face model, skull model, and safe zone model.

	Face Model	Skull Model	Safe Zone Model
20221116	(0.6, 1, 1)	(0.3, 1, 1)	(0.2, 1, 1)
20240806	(0.8, 1, 1)	(0.4, 1, 1)	(0.2, 1, 1)

difficulty of the cochlear implant surgery.

During cochlear implant surgery, a portion of soft tissue and bone structure must first be cut or removed to expose the round window, as shown in figure 6. Once the round window is accurately positioned, the surgeon can insert the electrode array of the cochlear implant into the inner ear structure through the round window, as shown in figure 5. This critical step is essential for the successful implantation of the cochlear implant and requires extreme caution during the operation to avoid damaging important tissue such as surrounding nerves and blood vessels.

After multiple threshold adjustments and effect previews, this paper optimizes the threshold settings of each CT data set during image segmentation. The specific setting values are shown in Table 2. When using the Cleaver method to construct the volumetric mesh, the author sets different feature scaling ratios, sampling rates, and rates of change of element size for the face model, skull model, and safe zone model in each CT dataset. For detailed parameters, see Table 3, where each set of triplets represents the feature scaling ratio, sampling rate, and rate of change of element size from left to right.

The setting of these parameters strikes a balance between accuracy and usability. Accuracy refers to the degree of detail presentation, while usability means that the calculation time of each simulated cutting operation during the simulation process should not be too long. The finer the volumetric mesh of the model is constructed, the larger the model is, and the longer the calculation time

Figure 21: Representative CT image of a normal left ear showing the basic anatomy of the ear structures, particularly the cochlea, from an axial view.

of each simulated cutting operation is. In addition, if the volumetric mesh is constructed too finely, it may cause 3D Slicer to return a build failure message, or even cause the computer to crash and automatically restart during the calculation process. Among the three models, the face model, the skull model and the safe zone model, the safe zone model requires the highest accuracy, while the face model requires the lowest accuracy. This difference is reflected in the parameter settings of the Cleaver method to ensure that each model meets the accuracy requirements while reducing the size of the model.

Figures 21, 22, 23, and 24 show representative CT images of a normal left ear, a normal right ear, an abnormal left ear, and an abnormal right ear, respectively, showing the basic anatomical morphology of the ear, especially the cochlear structure, from an axial view, providing necessary image references for simulation operations. Next, Figures 25a, 26a, 27a, and 28a show the overall views of the 3D ear models of the four cases before any cutting and drilling operations. These initial models present the complete external ear anatomical structure as the initial state of surgical simulation. Subsequently, in Figures 25b, 26b, 27b, and 28b, you can see the model view after removing some skin tissue. At this stage, more skin layers are removed and the bone structure is exposed, providing a clearer anatomical view for the subsequent drilling and cutting operations. Figures 25c, 26c, 27c, and 28c show that the round window structure is revealed after further removal of the exposed bone structure. This

Figure 22: Representative CT image of a normal right ear showing the basic anatomy of the ear structures, particularly the cochlea, from an axial view.

Figure 23: Representative CT image of a abnormal left ear showing the basic anatomy of the ear structures, particularly the cochlea, from an axial view.

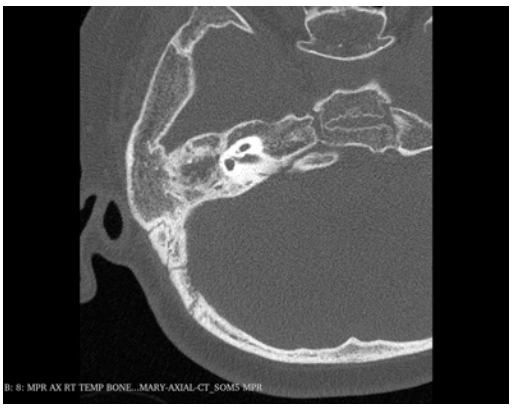

Figure 24: Representative CT image of a abnormal right ear showing the basic anatomy of the ear structures, particularly the cochlea, from an axial view.

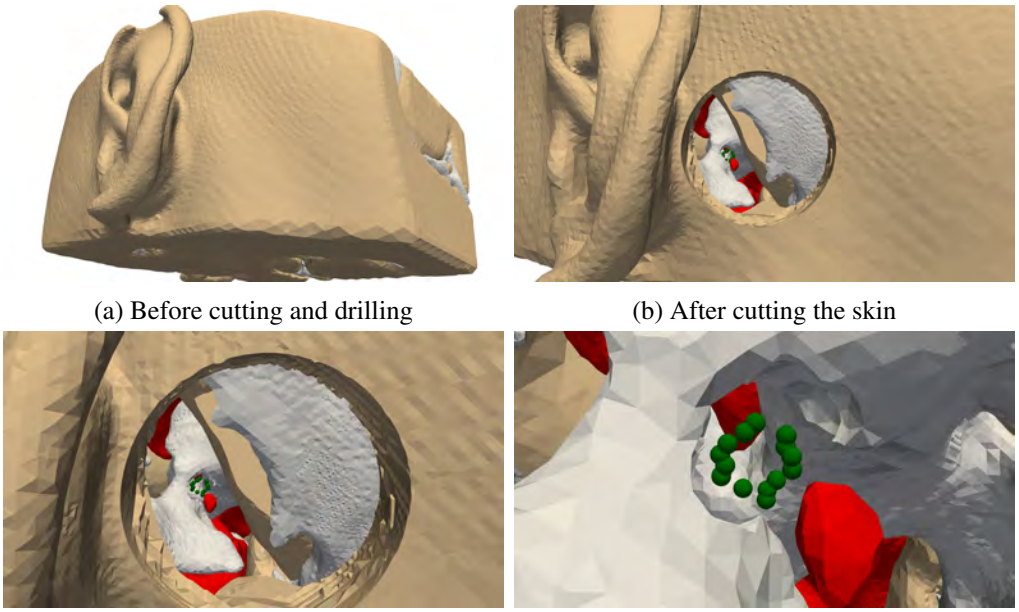

(a) Before cutting and drilling (b) After cutting the skin

(c) After cutting the skin and drilling the bone (d) Round window area

Figure 25: Schematic diagram of different cutting and drilling stages of the 3D normal left ear model **(a)** 3D ear model before cutting and drilling; **(b)** model after cutting the skin and removing soft tissue; **(c)** model after cutting the skin and drilling the bone to expose the round window; **(d)** enlarged view of the round window area in (c).

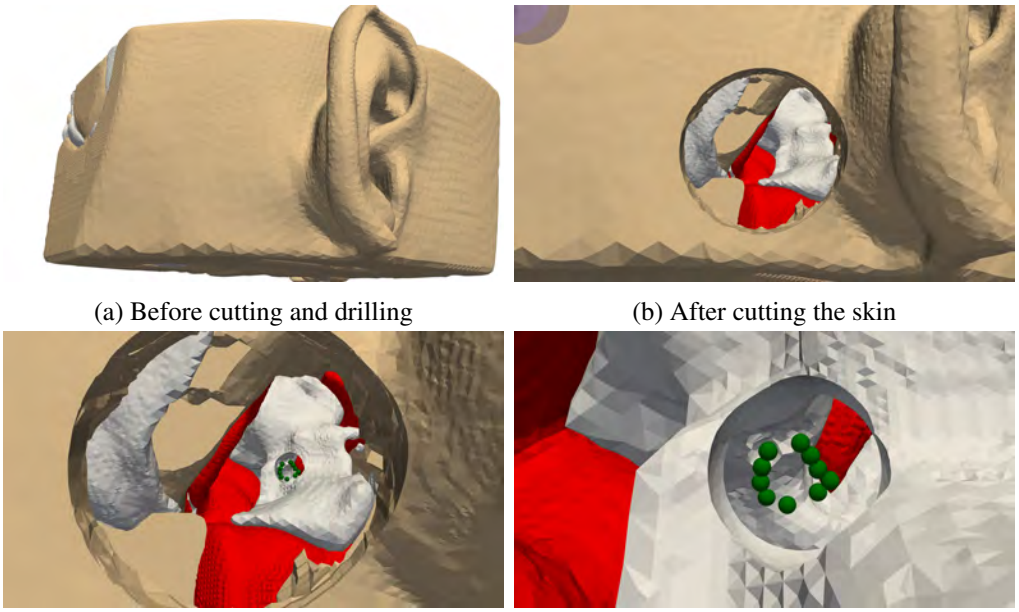

(a) Before cutting and drilling (b) After cutting the skin

(c) After cutting the skin and drilling the bone (d) Round window area

Figure 26: Schematic diagram of different cutting and drilling stages of the 3D normal right ear model **(a)** 3D ear model before cutting and drilling; **(b)** model after cutting the skin and removing soft tissue; **(c)** model after cutting the skin and drilling the bone to expose the round window; **(d)** enlarged view of the round window area in (c).

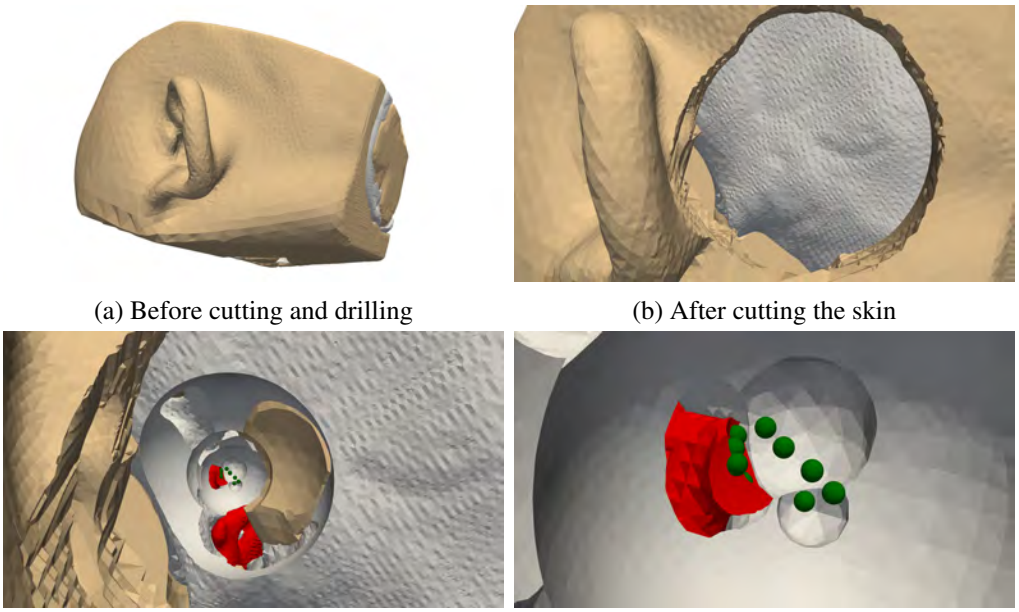

(a) Before cutting and drilling

(b) After cutting the skin

(c) After cutting the skin and drilling the bone

(d) Round window area

Figure 27: Schematic diagram of different cutting and drilling stages of the 3D abnormal left ear model **(a)** 3D ear model before cutting and drilling; **(b)** model after cutting the skin and removing soft tissue; **(c)** model after cutting the skin and drilling the bone to expose the round window; **(d)** enlarged view of the round window area in (c).

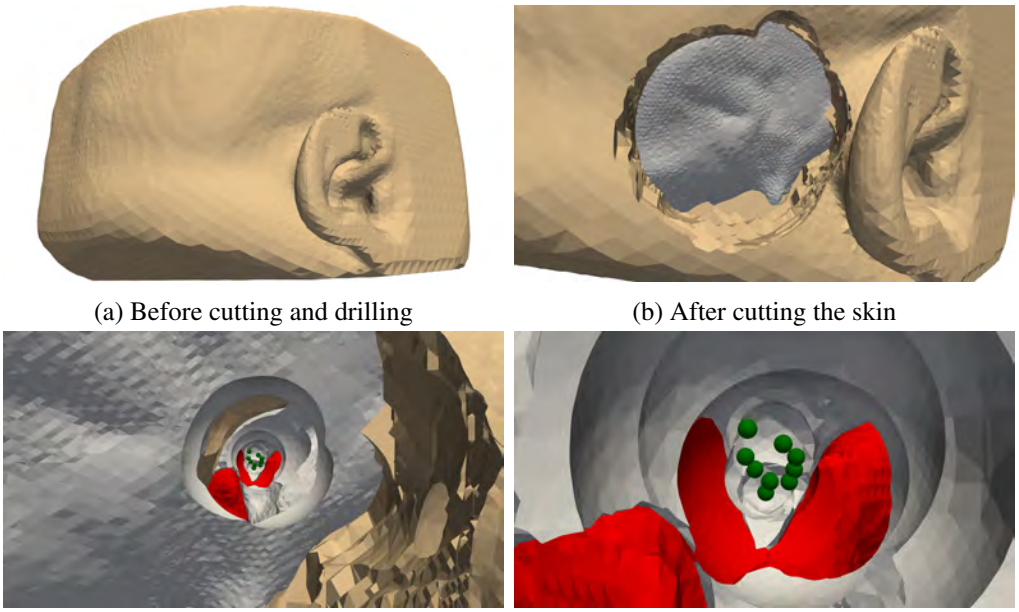

(a) Before cutting and drilling

(b) After cutting the skin

(c) After cutting the skin and drilling the bone

(d) Round window area

Figure 28: Schematic diagram of different cutting and drilling stages of the 3D abnormal right ear model **(a)** 3D ear model before cutting and drilling; **(b)** model after cutting the skin and removing soft tissue; **(c)** model after cutting the skin and drilling the bone to expose the round window; **(d)** enlarged view of the round window area in (c).

step simulates the bone drilling process during surgery, as close as possible to the anatomical effect shown in Figure 5. Finally, Figures 25d, 26d, 27d, and 28d are enlarged views of the round window, which further clearly show the final exposure state of the round window structure and provide intuitive visual support for subsequent electrode implantation. Through these step-by-step illustrations, this report fully reproduces the key processes of cutting and drilling in surgical simulation, providing a clear simulation demonstration of the ear anatomical structure and surgical methods.

Through experiment, this report found that for patients with normal ear anatomy, only a small amount of skin tissue and bone structure needs to be removed, and the round window structure can be clearly seen, as shown in the area surrounded by the green sphere in Figures 25d and 26d. This is because in normal anatomy, there is a large air cavity near the round window, which provides sufficient operating space for surgical instruments and smooths the operation.

On the contrary, for patients with abnormal anatomy, a large amount of skin tissue and bone structure need to be removed to expose the round window, as is shown in Figure 27d, and 28d. In addition, during the cutting process, surgical instruments can easily damage important tissue marked in red in the model, which include blood vessels and facial nerves. These anatomical features increase the complexity and risk of surgery.

The above simulation results show that the air cavities in the normal ear anatomy simplifies the surgical process, eases the exposure and operation of the round window. However, in the case of abnormal anatomical structure, the lack of these air cavities significantly increases the difficulty of surgery and requires more cautious operations and strategies.

In addition, during the reconstruction of the ear model, the number of axial CT slices available for marking the round window structure of patient 20240806 with abnormal ear anatomy was less than that of patient 20221116 with normal ear anatomy. This means that the round window structure of patient 20240806 is

smaller in size and the anatomical details are more complex, further increasing the difficulty of the surgery. Therefore, it is particularly necessary to use a simulator for surgical simulation before surgery, which helps surgeons to gain a deeper understanding of the patient's unique anatomical characteristics, develop more accurate surgical plans, and reduce surgical risks.

5 Future Work and Conclusions

The ear model reconstruction and surgical simulation tool in this report has been highly recognized by surgeons, who believe that the tool will be of great help in the surgical process.

In the later stages of this project, the author obtained high-resolution CT images of patients 20221116 and 20240806, but due to time constraints, only the ear modeling has been completed. In the future, the author plans to integrate the ear model with the overall skull model to build a multi-resolution model. By using higher resolution modeling for important areas and lower resolution modeling for secondary areas, the accuracy of the simulation can be guaranteed while ensuring the usability of the simulation tool and avoiding long calculation time for each step.

To better segment fine structures, the author will improve image segmentation and modeling methods. In the simulator software developed in this report, a menu bar can be added in the future to provide more abundant operation options. The cutting calculation will adopt a multi-threaded mechanism to further improve the response speed and enable the software to run smoothly on more sophisticated models. For illegal user operations, such as setting the cutting radius to a negative value, the author plans to provide more friendly exception information prompts instead of the current pop-up window that directly displays the code exception information. This will improve the user experience and avoid unnecessary confusion.

In addition, the author notes that Celeste R.C. Poley has developed a new path planning algorithm that combines rapidly exploring random trees (RRT) and sequential quadratic programming (SQP) to improve the safety of cochlear implant surgery[31]. In the future, the author hopes to integrate this path planning algorithm into simulation software to provide doctors with accurate path planning suggestions, consequently optimizing the surgical process and ensuring patients' safety.

In general, this report successfully used actual CT images to build an ear model based on individual patients and developed a drilling simulator that supports simultaneous import, rendering, interaction, and cutting of face, skull, safe zone models, and landmarks. Through simulation experiments on different patients, it was found that patient-specific models can more accurately reflect the anatomical characteristics of the ear and help identify difficulties that may be encountered during surgery. Especially for patients with abnormal anatomical structures, simulation tools can help surgeons identify potential risks in advance, optimize surgical plans, and ensure the safety and effectiveness of surgery. The results of this report have good application prospects in preoperative planning and surgical simulation of cochlear implant surgery. Future improvements will further enhance its application value and provide strong support for improving the success rate of surgery and patient prognosis.

Bibliography

[1] Carrie L. Nieman, Emmanuel E. Garcia Morales, Alison R. Huang, Nicholas S. Reed, Sevil Yasar, and Esther S. Oh. Prevalence of hearing loss and hearing aid use among persons living with dementia in the us. *JAMA Network Open*, 7(10):e2440400, October 2024.

[2] Adebola Stephen Oluwatosin, Ogunleye Oluwaseun Olayinka, and Adeyemo Adebolajo Adeyemo. Classification of hearing status and health-related quality of life of elderly people with presbycusis in south-west, nigeria. *International Journal of Otolaryngology*, 2020:6459276, 2018.

[3] Regina Klas and Adriana Lacerda. The audiometric findings among curitiba and metropolitan area students. *International Archives of Otorhinolaryngology*, 18(2):165–171, April 2014.

[4] Margaret Zuriekat, Sireena Qarmout, Malak Alsous, Amani Nanah, Fares Al-Halasa, Safa Alqudah, and Sara Alhanbali. Hearing loss in jordan: an overlooked public health challenge. *Jordan Medical Journal*, 2024.

[5] Frank R. Lin, Kristine Yaffe, Jin Xia, Qian-Li Xue, Tamara B. Harris, Elizabeth Purchase-Helzner, Suzanne Satterfield, Hilsa N. Ayonayon, Luigi Ferrucci, and Eleanor M. Simonsick. Hearing loss and cognitive decline in older adults. *JAMA Internal Medicine*, 173(4):293–299, February 2013.

[6] Hui-Fu Wang, Wei Zhang, Edmund T. Rolls, Yuzhu Li, Linbo Wang, Ya-Hui Ma, Jujiao Kang, Jianfeng Feng, Jin-Tai Yu, and Wei Cheng.

Hearing impairment is associated with cognitive decline, brain atrophy and tau pathology. *eBioMedicine*, 86, December 2022. doi: 10.1016/j.ebiom.2022.104336.

[7] Thomas D Parker, Chris Hardy, Sarah Keuss, William Coath, David M Cash, Kirsty Lu, Jennifer M Nicholas, Sarah-Naomi James, Carole Sudre, Sebastian Crutch, Doris-Eva Bamiou, Jason D Warren, Nick C Fox, Marcus Richards, and Jonathan M Schott. Peripheral hearing loss at age 70 predicts brain atrophy and associated cognitive change. *Journal of Neurology, Neurosurgery & Psychiatry*, 95(9):829–832, 2024.

[8] Kurtis Young, Maeher R. Grewal, Rodney C. Diaz, Arthur W. Wu, and Mia E. Miller. Cochlear implantation after stereotactic radiosurgery for vestibular schwannoma: Initial hearing improvement and longevity of hearing restoration. *Otol Neurotol*, 44(3):201–208, March 2023.

[9] Dayse Távora-Vieira, Roberta Marino, Aanand Acharya, and Gunesh P. Rajan. The impact of cochlear implantation on speech understanding, subjective hearing performance, and tinnitus perception in patients with unilateral severe to profound hearing loss. *Otol Neurotol*, 36(3):430–436, March 2015.

[10] Christiane Völter, Lisa Götze, Imme Haubitz, Janine Müther, Stefan Dazert, and Jan Peter Thomas. Impact of cochlear implantation on neurocognitive subdomains in adult cochlear implant recipients. *Audiology & Neurotology*, 26(4):236–245, 2021 2021.

[11] Miryam Calvino, Isabel Sánchez-Cuadrado, Javier Gavilán, M. Auxiliadora Gutiérrez-Revilla, Rubén Polo, and Luis Lassaletta. Effect of cochlear implantation on cognitive decline and quality of life in younger and older adults with severe-to-profound hearing loss. *European Archives of Oto-Rhino-Laryngology*, 279(10):4745–4759, October 2022.

[12] Jonas Jeppesen and Christian Emil Faber. Surgical complications following cochlear implantation in adults based on a proposed reporting consensus. *Acta Oto-Laryngologica*, 133(10):1012–1021, October 2013.

[13] Neal P. Dillon, Ramya Balachandran, and Robert F. Labadie. Accuracy of linear drilling in temporal bone using drill press system for minimally invasive cochlear implantation. *International Journal of Computer Assisted Radiology and Surgery*, 11(3):483–493, March 2016.

[14] Ramya Balachandran, Jason E. Mitchell, Grégoire Blachon, Jack H. Noble, Benoit M. Dawant, J. Michael Fitzpatrick, and Robert F. Labadie. Percutaneous cochlear implant drilling via customized frames: an in vitro study. *Otolaryngology–Head and Neck Surgery*, 142(3):421–426, March 2010.

[15] Robert F. Labadie, Ramya Balachandran, Jack H. Noble, Grégoire S. Blachon, Jason E. Mitchell, Fitsum A. Reda, Benoit M. Dawant, and J. Michael Fitzpatrick. Minimally invasive image-guided cochlear implantation surgery: first report of clinical implementation. *The Laryngoscope*, 124(8):1915–1922, August 2014.

[16] Lena Geiger, M. Geraldine Zuniga, Thomas Lenarz, Omid Majdani, and Thomas S. Rau. Drilling accuracy evaluation of a mouldable surgical targeting system for minimally invasive access to anatomic targets in the temporal bone. *European Archives of Oto-Rhino-Laryngology*, 280(10):4371–4379, October 2023.

[17] S. Raghunandhan, Mohan Kameswaran, R. S. Anand Kumar, Anoop Kumar Agarwal, and Mohammod Delwar Hossain. A study of complications and morbidity profile in cochlear implantation: The merf experience. *Indian Journal of Otolaryngology and Head & Neck Surgery*, 66(Suppl 1):161–168, January 2014.

[18] Nick Saunders. Perforated ear drum, 2024. Accessed: 2024-11-08.

[19] Encyclopaedia Britannica. Cochlear nerve and central auditory pathways, 2024. Accessed: 2024-11-08.

[20] Jackler and Gralapp. Cochlear implant surgery. Accessed: 2024-11-09.

[21] Jackler and Gralapp. Cochlear implant surgery. Accessed: 2024-11-09.

[22] Peter Trier, Karsten Østergaard Noe, Mads Sølvsten Sørensen, and Jesper Mosegaard. The visible ear surgery simulator. *Studies in Health Technology and Informatics*, 132:523–525, 2008.

[23] Blake Jones, Seyed Alireza Rohani, Nelson Ong, Tarek Tayeh, Ahmad Chalabi, Sumit K. Agrawal, and Hanif M. Ladak. A virtual-reality training simulator for cochlear implant surgery. *Simulation & Gaming*, 50(2):243–258, 2019.

[24] Rebecca L. Turok, Robert F. Labadie, George B. Wanna, Benoit M. Dawant, and Jack H. Noble. Cochlear implant simulator for surgical technique analysis. In Ziv R. Yaniv and David R. Holmes III, editors, *Medical Imaging 2014: Image-Guided Procedures, Robotic Interventions, and Modeling*, volume 9036, page 903619. International Society for Optics and Photonics, SPIE, 2014.

[25] Mario Ceresa, Nerea Mangado Lopez, Hector Dejea Velardo, Noemi Carranza Herrezuelo, Pavel Mistrik, Hans Martin Kjer, Sergio Vera, Rasmus R. Paulsen, and Miguel Angel González Ballester. Patient-specific simulation of implant placement and function for cochlear implantation surgery planning. In Polina Golland, Nobuhiko Hata, Christian Barillot, Joachim Hornegger, and Robert Howe, editors, *Medical Image Computing and Computer-Assisted Intervention – MICCAI 2014*, pages 49–56, Cham, 2014. Springer International Publishing.

[26] Olivier Goury, Yann Nguyen, Renato Torres, Jeremie Dequidt, and Christian Duriez. Numerical simulation of cochlear-implant surgery: Towards patient-specific planning. In Sebastien Ourselin, Leo Joskowicz, Mert R. Sabuncu, Gozde Unal, and William Wells, editors, *Medical Image Computing and Computer-Assisted Intervention – MICCAI 2016*, pages 500–507, Cham, 2016. Springer International Publishing.

[27] Paolo Cignoni, Massimiliano Corsini, and Guido Ranzuglia. Meshlab: an open-source 3d mesh processing system. *ERCIM News*, 2008, 2008.

[28] CIBC, 2015. Cleaver: A MultiMaterial Tetrahedral Meshing Library and Application. Scientific Computing and Imaging Institute (SCI), Download from: http://www.sci.utah.edu/software.html.

[29] Jonathan R. Bronson, Joshua A. Levine, and Ross T. Whitaker. Lattice cleaving: Conforming tetrahedral meshes of multimaterial domains with bounded quality. *Proceedings of the International Meshing Roundtable*, pages 191–209, 2013.

[30] Hang Si. Tetgen, a delaunay-based quality tetrahedral mesh generator. *ACM Trans. Math. Softw.*, 41(2), February 2015.

[31] Celeste RC Poley. *Cochlear Implantation: Path Planning Algorithms and Dynamics*. PhD thesis, University of Maryland, College Park, 2022.